nature chemistry

ARTICLES

PUBLISHED ONLINE: 15 JUNE 2015 | DOI: 10.1038/NCHEM.2280

Through-space transfer of chiral information mediated by a plasmonic nanomaterial

Saeideh Ostovar pour[1], Louise Rocks[2], Karen Faulds[2], Duncan Graham[2], Václav Parchaňský[3,4], Petr Bouř[3,4]* and Ewan W. Blanch[1,5]*

The ability to detect chirality gives stereochemically attuned nanosensors the potential to revolutionize the study of biomolecular processes. Such devices may structurally characterize the mechanisms of protein–ligand binding, the intermediates of amyloidogenic diseases and the effects of phosphorylation and glycosylation. We demonstrate that single nanoparticle plasmonic reporters, or nanotags, can enable a stereochemical response to be transmitted from a chiral analyte to an achiral benzotriazole dye molecule in the vicinity of a plasmon resonance from an achiral metallic nanostructure. The transfer of chirality was verified by the measurement of mirror image surface enhanced resonance Raman optical activity spectra for the two enantiomers of both ribose and tryptophan. Computational modelling confirms these observations and reveals the novel chirality transfer mechanism responsible. This is the first report of colloidal metal nanoparticles in the form of single plasmonic substrates displaying an intrinsic chiral sensitivity once attached to a chiral molecule.

Nanosculptured materials with chiral plasmonic properties[1–3] have recently attracted attention due to their ability to generate broadband circular polarization states in light, as well as superchiral electromagnetic fields for the ultrasensitive detection of biomolecular conformation[4]. Plasmonic nanomaterials such as metallic nanoparticles exhibit strong extinction in the visible wavelength range, but are achiral, with no inherent chiroptical properties[1–3]. It has previously been demonstrated that when biomolecules are assembled with nanomaterials, chirality from the biomolecule can be imparted to the nanomaterial, resulting in the generation of a plasmon-induced circular dichroism (CD) signal in the visible spectral region[4]. This has been investigated for a limited number of chiral biomolecule/nanomaterial complexes, examples of which include DNA[5] and peptide nanotubes decorated with gold or silver nanoparticles[6–8]. The optical chirality of nanostructured systems is therefore a field of active research, with potential applications in optically active devices for biomedical science, environmental sensing and bioterrorism detection. It has also been shown that chiral patterns can be formed by both chiral and achiral molecules[9]. The phenomenon of induced chirality at a surface, observed through mirror-symmetry breaking upon molecular adsorption and transfer of handedness, has also been investigated[10]. This chirality induction can occur either from chiral molecules to a non-chiral surface or from a chiral surface to non-chiral molecules. Many achiral molecules have been reported to become chiral upon adsorption on a surface[11], while breaking of the mirror symmetry of chiral molecules once adsorbed on surfaces can induce a chiral footprint on the surface[10].

Single nanoparticle plasmonic substrates, such as hollow gold nanospheres[12], silver triangles[13], gold nanorods[14] and gold/silver silica nanoshells[15], have localized surface plasmon resonances that match the excitation wavelengths of lasers used in, for example, Raman spectroscopy. They provide a strong electromagnetic field that increases the Raman cross-section (which is a measure of the Raman signal intensity generated per molecule), giving rise to surface-enhanced Raman scattering (SERS), and thus represent a more stable and more manageable alternative to the high conjunction potentials or 'hot spots' that are characteristic of aggregated metal colloids. Additionally, they provide large scattering cross-sections that allow colorimetric detection of analytes at relatively low concentrations[16].

Colloidal suspensions of silver nanoparticles that have been functionalized with dyes, such as azo-functionalized benzotriazoles, and then coated in a silica shell, act as single plasmonic substrates with

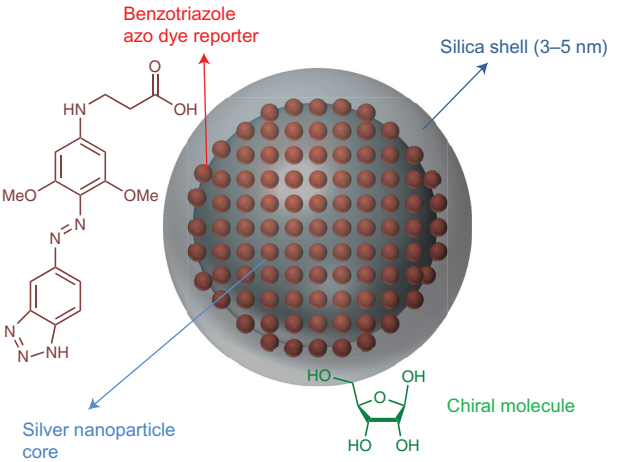

Figure 1 | Schematic of the silver nanotag. The silver nanoparticle core is coated in a 3–5 nm silica shell, to which the benzotrizaole reporter and the chiral analyte are bound.

[1]Faculty of Life Sciences and Manchester Institute of Biotechnology, University of Manchester, 131 Princess Street, Manchester M1 7DN, UK. [2]Centre for Molecular Nanometrology, WestCHEM, Department of Pure and Applied Chemistry, University of Strathclyde, Glasgow G1 1XL, UK. [3]Department of Analytical Chemistry, University of Chemistry and Technology, Technická 5, Prague 16628, Czech Republic. [4]Institute of Organic Chemistry and Biochemistry, Academy of Sciences, Flemingovo náměstí 2, Prague 16610, Czech Republic. [5]School of Applied Sciences, RMIT University, GPO Box 2476, Melbourne VIC 3001, Australia. *e-mail: bour@uochb.cas.cz; ewan.blanch@rmit.edu.au; e.blanch@manchester.ac.uk

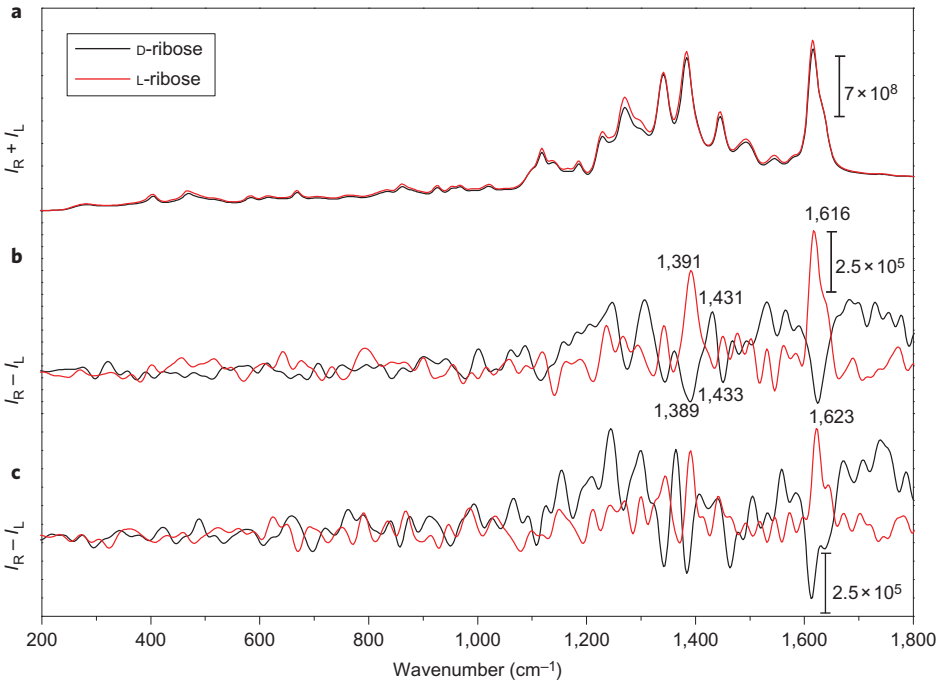

Figure 2 | SERRS spectra and SERROA spectra. a–c, SERRS spectra of D- and L-ribose attached to silver silica nanotags (**a**) and SERROA spectra of D- and L-ribose for replicate experiments (**b**,**c**), illustrating the level of reproducibility, with a data collection time of 35 min and laser power at source of 0.20 W. Identical SERRS spectra are observed for D- and L-ribose, because SERRS is blind to chirality, while mirror image SERROA bands are measured for the two enantiomers, signifying the chiroptical sensitivity of these nanotags.

an electronic absorption profile that can be tuned to the excitation frequency of the laser[17]. These single nanoparticle plasmonic substrates can detect and provide useful information about biomolecules based on vibrational information. However, there have been no previous reports regarding their propensity to have any chiroptical activity. In this Article we demonstrate the optical activity of these plasmonic substrates in the form of resonant dye molecule-labelled nanoprobes, using Raman optical activity (ROA) spectroscopy. ROA measures the intensity difference between Raman scattering in left- and right-circularly polarized light from chiral molecules[18–21]. No ROA signals are detected for racemic mixtures or if a molecule possesses a plane or centre of symmetry, but spectral bands of opposing sign are detected for enantiomers[22].

Here, we report the observation of such chiroptical behaviour induced in silver silica nanotags with an achiral structure. Furthermore, we show that chirality is induced into the achiral plasmonic surface of the substrate by enantiomeric analytes. This is a new phenomenon of chirality induction that is fundamentally different to previously reported mechanisms[23–29]. We observe a symmetry breaking of surface plasmons interacting with a resonant dye molecule once they are tethered to chiral molecules. Both the silver nanoparticles, which provide the surface plasmons, and the dye molecules adsorbed onto the surface remain non-chiral. Once the dye molecule-labelled nanotags capture chiral molecules, in this case enantiomers of ribose and tryptophan, they become chiroptically active. The handedness of the ribose and tryptophan enantiomers was transferred into the surface plasmon layer, resulting in opposing mirror image responses of the achiral dye reporter in the ROA spectra for the different enantiomers.

Results and discussion

Silver silica nanotags were linked with benzotriazole azo dye molecules (Fig. 1) to construct surface enhanced resonant Raman spectroscopic (SERRS) nanoprobes designed to provide a maximum enhancement at ~514 nm (ref. 17). These dyes can act as both a resonant reporter for SERRS and a precursor for the formation of silica shells, which stabilize the silver nanoparticle cores. The optical responses of the dye-labelled nanotags were first characterized[30,31], and their SERRS spectra both with and without the silica nanoshell coating are shown in Supplementary Fig. 4a,b. Their identical SERRS profiles, with strong bands originating from the dye, show that the silica shell does not interfere with the dye's SERRS signal. Corresponding surface enhanced resonant Raman optical activity (SERROA) spectra of silver nanotags with and without a silica nanoshell (Supplementary Fig. 4c,d) also show similar spectral features being dominated by positive bands. The positive SERROA bands resemble the parent SERRS bands, but with a lower signal-to-noise ratio, which indicates in both cases that the observed bands principally originate from the interaction of linear contaminants in the scattered circularly polarized light with the SERRS bands. We therefore conclude that these particular bands are not SERROA signals but residual artefacts, a common problem in attempts to measure the SERROA effect that necessitates careful characterization of the interaction between the surface plasmons and circularly polarized radiation[31,32]. The weak features present in Supplementary Fig. 4c,d between 200 and 1,100 cm^{-1} indicate the noise level of these measurements.

Figure 2 presents the SERRS and SERROA spectra of L- and D-ribose covalently attached to the silver silica nanotags. The SERRS spectra of the two enantiomers of ribose have identical profiles to one another, as well as to the SERRS spectra of the silver silica nanotags (Supplementary Fig. 4), because the resonance effect of the bound benzotriazole dye dominates the spectra. The SERS spectra of L- and D-ribose reported previously[30] are significantly different from the SERRS spectra measured for the same analytes here, because the previous study measured the direct interaction of the ribose molecules with the metal nanoparticle surfaces, which is not the case for this study. Here, the SERRS spectra are dominated by the characteristic bands of the benzotriazole dye molecules. Once the experimental conditions were optimized, the measured spectra

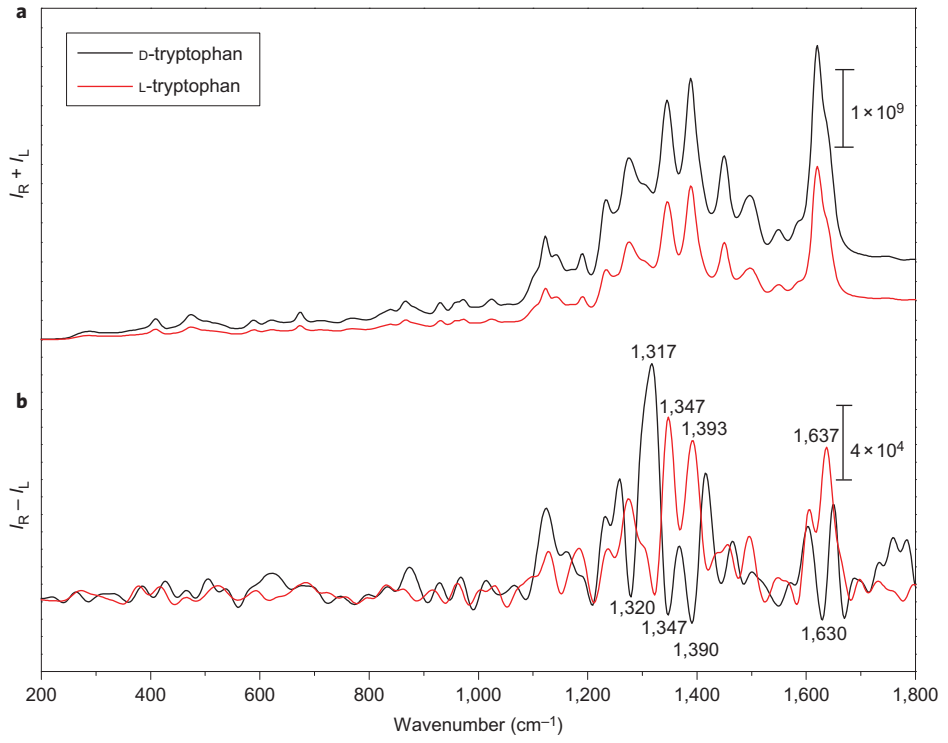

Figure 3 | SERRS spectra and SERROA spectra. a,**b**, SERRS spectra of D- and L-tryptophan attached to silver silica nanotags (**a**) and SERROA spectra of D- and L-tryptophan (**b**), with a data collection time of 35 min and laser power at source of 0.20 W. The nanotags also show strong chiroptical responses in the SERROA spectra of L- and D-tryptophan.

showed good reproducibility for all spectral bands shown. Each batch of nanotags was stable for at least one month.

Chiroptical response. Crucially, the corresponding SERROA spectra presented in Fig. 2b,c for D- and L-ribose exhibit a strong mirror image response and with very different features to their corresponding SERRS bands, unlike the already discussed (Supplementary Fig. 4) spectra obtained from the achiral silver silica nanotags. It is clear that the SERROA spectra for the two enantiomers of ribose contain both positive and negative bands, the positions of which correlate well with each other. The circular intensity difference, or ROA/Raman signal ratio, is $\sim 4 \times 10^{-4}$ for the main SERROA bands in both cases, quantitatively verifying the mirror image response. Strong peaks appearing in the region above 1,200 cm^{-1} in both SERROA spectra are clearly resolved from the background noise, verifying the detection of the chiroptical response in the presence of L- or D-ribose, which then confirms the stereochemistry of each analyte. For example, the strong +ve/−ve/+ve SERROA bands at 1,391, 1,431 and 1,450 cm^{-1} for L-ribose correspond to the −ve/+ve/−ve bands at 1,389, 1,433 and 1,450 cm^{-1} for the D-enantiomer. In addition, the strongest SERROA bands at 1,616 and 1,623 cm^{-1} for L- and D-ribose, respectively, also have opposite signs. The differences in the band positions can be attributed to experimental noise and the limited precision of the charge-coupled device detector. The fact that the observed SERROA bands correspond to the SERRS bands from the benzotriazole dye rather than from the intrinsic surface enhanced Raman optical activity (SEROA) signals previously reported for L- and D-ribose[33] suggests that we are observing the effect of ribose chirality on the plasmon at the silver nanotag surface as it modifies the surface state. This chiral response is then imprinted on the SERRS spectrum of the benzotriazole dye, leading to the enantiomeric sensitivity observed for the SERROA bands.

To further verify these results, the SERRS and SERROA spectra of another enantiomeric pair, L- and D-tryptophan, were also measured, and are presented in Fig. 3. Indeed, as before, the SERRS profiles for both enantiomers are identical to those found for the benzotriazole dye-tagged silver colloids. The corresponding SERROA spectra for the two enantiomers of this amino acid again display mirror image responses, in particular at 1,317, 1,347 and 1,390 cm^{-1}, which are associated with corresponding SERRS bands from the benzotriazole nanotags. Although the SERROA spectral profiles are similar for ribose and tryptophan, the intensities for ribose are significantly stronger than for tryptophan. As ROA intensities are sensitive to conformational dynamics, this suggests that the SERROA signal is also quantitatively sensitive to the greater rigidity of the cyclic ribose molecule compared to the more flexible amino acid. More mirror image bands are observed for L- and D-ribose than for L- and D-tryptophan within the region of 1,400–1,600 cm^{-1}, such as at 1,531 and 1,564 cm^{-1}, which correlates with the superior signal-to-noise ratios obtained for ribose.

Computational modelling verifies our experimental results. The experimental results are in good agreement with our modelling of the chiral response of the nanoplasmonic system once a chiral analyte is introduced. In particular, although under non-resonance conditions both ribose and some chiral conformations of the dye have distinct ROA and Raman spectra, in a complex both spectral intensities start to be dominated by the dye's vibrational bands. Our calculations verify that the chiral analyte induces a chiral response in the resonant Raman spectrum of the achiral benzotriazole dye. The SERRS and SERROA spectra simulated for the most complex model we used are plotted in Fig. 4. For the dye, a smaller, arbitrarily symmetrized (of C_s symmetry) analogue was used to avoid conformational averaging and to represent its inherently achiral character. Control computations show that the electronic and vibrational spectral features correspond well to those of the fully functionalized benzotriazole. A ribose molecule was then placed nearby, with the centre of mass in the dye's plane and the colloid represented by a

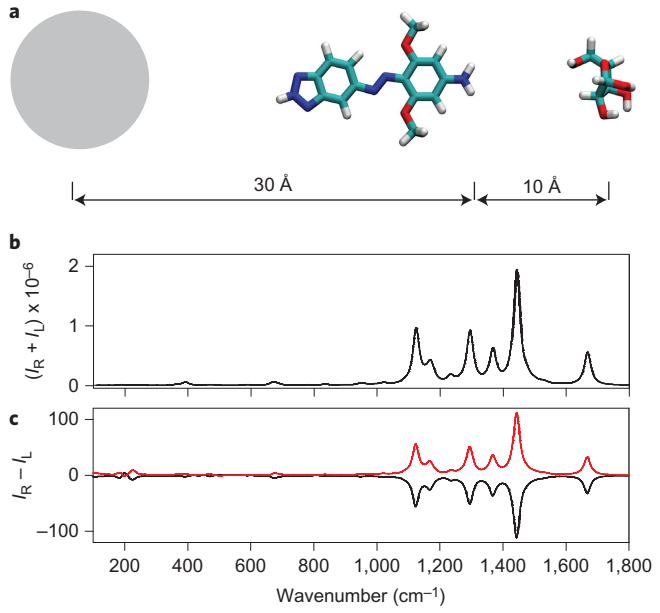

Figure 4 | Model system and its Raman and ROA spectra, generated by matrix perturbation theory. a, The colloid is represented by a polarizable sphere (with isotropic polarizability $\alpha = 10^5$ a.u.). For the simplified dye and ribose molecule the ROA tensors were calculated at the B3LYP/6-31G* (SMD) level at an excitation frequency of 532 nm and averaged over the ribose rotation around its mass centre. **b**,**c**, The modelled SERRS spectra for D- and L-ribose overlap perfectly (**b**), while the DFT model verifies that the stereochemically sensitive SERROA bands (**c**) originate from vibrations of the benzotriazole dye molecule.

polarizable sphere. Spectra averaged over 64 ribose orientations were then plotted. Interestingly, both the orientational averaging and the presence of the colloid had only a minor effect on the results. Most significantly, the modelled SERROA intensities are dominated by the bands coming from the dye vibrations. The vibrational bands from ribose are invisible at this scale; they may, however, mix with those of the dye for different resonance conditions. In a near resonance the simulated SERROA signal for a particular ribose enantiomer is of one sign only, as it should be for the single electronic state limit[34,35]. The role of the ribose in the induction of optical activity thus appears to be perturbation of the dye molecule's symmetry, or, in experiments, in perturbation of the average spherical symmetry of the nanotag.

The observation of mirror image SERROA bands for the benzotriazole dye can thus be explained on the basis that chiral molecules, in this study L- and D-ribose or L- and D-tryptophan, once attached to the nanoprobe possess the enantioselectivity required to break the symmetric environment of the achiral metallic cluster. This is reported here by the SERRS response from the dye molecules, which are in close proximity to the surface plasmons. In other words, induced dissymmetry in the surface plasmon interaction with the benzotriazole molecules is responsible for the observed mirror image bands in the SERROA spectra of L- and D-ribose and L- and D-tryptophan. Therefore, the induced SERROA phenomenon measured here is fundamentally different from that responsible for our previously reported SEROA spectra of L- and D-ribose[30] and the SERROA spectra of two resonant proteins myoglobin and cyctochrome c[36], because the direct interaction between the chiral molecules and the surface plasmons from metal nanoparticles in those cases was responsible for the enhancement of ROA signals. The SEROA spectral details in those previous studies also originate directly from the analyte investigated, whereas in the SERROA spectra presented in this study we observe the transfer of a chiral influence from the analyte onto the SERRS spectrum of the achiral benzotriazole dye. Chirality observed in the former systems mainly originates from dipolar interactions with chiral molecules[36]. Our current observation of chiroptical behaviour monitored by dye-labelled nanotags is principally due to radiative electromagnetic coupling between the surface plasmons generated by these nanotags and the surrounding chiral molecules interacting over a long range[37]. The chiral perturbation existing in the presence of achiral chromophores has induced optical activity to the metal nanoparticles and the dye, both of which act as agents enhancing the Raman signal, the former via surface plasmons, the latter via electronic resonance.

A new form of chirality transfer. The mechanism proposed as being responsible for these SERROA results can be compared to the mechanism recently reported for a class of hybrid plasmonic nanomaterials[37] sensitive to indirect adsorption of chiral molecules. Abdulrahman and colleagues[37] demonstrated that a chiral response was induced into the plasmonic resonance of the achiral nanostructure using CD, by measurement of electronic excitation through the radiative electromagnetic interaction between a non-absorbing isotropic chiral medium and a strongly absorbing metallic plasmon resonance. In this Article we have also observed an induced chiral response, but by monitoring vibrational excitation and without the requirement for a superchiral field. In the present case, the plasmon resonance from the silver surface induces the SERRS signal from the tethered benzotriazole dye molecules, with the chiral analyte then interacting with that SERRS signal to generate an enantiomerically sensitive response. The respective results from these two studies for tryptophan are revealing: Abdulrahman and colleagues reported no chiral response for tryptophan, while Fig. 3 clearly shows the chiral response evident for the same amino acid when tethered to our nanotags. Therefore, although our results involve a long-range interaction, in common with the $1/d$ dependence reported by Abdulrahman *et al.*, our observed chiral response cannot be explained by their radiative coupling mechanism.

Cao and colleagues reported a through-bond mechanism of chirality transfer for CD measurements on chiral 2-amino-3-phenylpropane-1-thiol ligands directly bound to gold surfaces[38], after specifically ruling out a through-space coupling as being responsible for their observations. In contrast, our modelling shows that a through-bond mechanism is not responsible for our SERROA results, and our chiral analyte is around 50 bonds from the metal surface, confirming that our chirality transfer phenomenon is a fundamentally different process to that reported by Cao and co-authors. Chirality transfer is a broad topic, and our results also appear to fundamentally differ from the electro-magnetic field (EM)-induced torsional perturbations in metamaterials consisting of pairs of split Cu-rings, which was reported by Liu and colleagues[39], and also from the transmission of chirality from single surface-bound molecules to complex chiral arrays through increasing molecular coverage on an ordered Cu(111) surface, as observed by Iski and co-authors[40].

These results clearly show that SERROA bands of opposing sign are obtained from the two enantiomers of chiral molecules and that these are signatures of a novel stereochemically sensitive nature from the long-range interactions between chiral molecules and the surface plasmons of these achiral dye-tagged nanoprobes. Comparison of this work with other recent reports of chirality transfer clarifies that we have observed a distinct and new process. Extension of these studies to other analytes and nanotag designs is expected to shed further light on this exciting new chiroptical phenomenon.

Methods

Synthesis of EDTA-reduced silver colloid (AgEDTA). Silver nanoparticles (diameter of ~40 nm) were synthesized according to the procedure described by

Fabrikanos and co-workers[41]. Briefly, sodium hydroxide (0.4 M, 10 ml) was injected into a boiling 1 l solution of EDTA (1.62×10^{-4} M). Silver nitrate (0.026 M, 10 ml) was added to the boiling solution in 2.5 ml aliquots. Following 15 min of continued heating, the solution was allowed to equilibrate to room temperature. Stirring was maintained throughout. The characterization of the conjugated nanoparticles is presented in Supplementary Section 'Characterisation of conjugated nanoparticles'.

Conjugation of dye to silver nanoparticles. Three separate replicates of nanoparticle–dye conjugates were synthesized for analysis. The tri-functional benzotriazole dye shown in Fig. 1 was added to AgEDTA (1 ml, 1.00×10^{-10} M) to a final concentration of 10^{-7} M. Samples were agitated before centrifugation (6,000 r.p.m., 20 min) and resuspended in 500 µl dH_2O.

Silica encapsulation of silver–precursor conjugates. Silica-encapsulated silver nanotags were synthesized following the method outlined by Graham and co-authors[17]. The nanoparticle–dye conjugates were prepared to 1 ml with the slow addition of ethanol. Silica growth was initiated by the addition of triethylamine (10 µl, 1% vol/vol in ethanol) and the sequential addition of tetraethyl orthosilicate (TEOS) (10 µl, 4% vol/vol in ethanol) over a 3 h period until the final concentration of TEOS was 5.4 mM.

Functionalization of silica-encapsulated nanotags. Based on the original nanoparticle concentration, the nanotags were functionalized with ~4,000× molar excess of the selected enantiomer, L- or D-, of the analyte, ribose or tryptophan. This was achieved by reacting 1.21 molar equivalents of triethoxysilylpropyl isocyanate with the required enantiomer—L- or D-ribose, or L- or D-tryptophan—in $NaHCO_3$ buffer (0.1 M at pH 9) at 4 °C overnight. The 'silanized' molecules were added to unwashed nanotags and agitated before centrifugation (7,000 r.p.m., 20 min) and resuspension (500 µl dH_2O). Due to the formation of dimers, trimers and possibly small aggregates, it was difficult to determine the actual nanotag:analyte molar ratio, so a 1:500 ratio is quoted based on the initial nanoparticle concentration used to prepare each sample. Figure 1 presents a schematic structure of the functionalized nanotags.

All Raman and ROA spectra were measured using a ChiralRaman spectrometer (BioTools) configured in the backscattering geometry and operating at a wavelength of 532 nm and with a spectral resolution of 7 cm^{-1}. The laser power was set to 0.20 W, with a laser power at the sample of ~0.10 W and data acquisition times ranging from 5 min to 2 h.

Model computations. To investigate various factors important for the chirality transfer, we performed a number of density functional theory (DFT) computations on simplified models including the dye and chiral analyte molecules. The B3LYP[42] functional and standard 6-311++G** basis set were applied, within the Gaussian software environment[43]. The universal solvation model (SMD)[44] was used to mimic the aqueous environment. Harmonic force field and frequency-dependent molecular polarizabilities needed to generate the Raman and ROA intensities[33] were generated for the excitation wavelength of 532 nm, to simulate the near-resonance conditions. Matrix perturbation theory[45] was used to generate the spectra of a silver-dye–L-ribose complex, from the polarizability tensors obtained from Gaussian. The spectra were generated using Lorentzian profiles with a full-width at half-height of 10 cm^{-1}.

Data. Research data associated with this Article will become available at the following link from July 2015: https://pure.strath.ac.uk/portal/en/projects/doctoral-training-grant-2008–ra4346%2827114569-e902-4216-90d1-a745eb78bdb1%29.html

Received 28 January 2015; accepted 12 May 2015; published online 15 June 2015

References

1. Gansel, J. K. *et al.* Gold helix photonic metamaterial as broadband circular polarizer. *Sci. Am.* **325,** 1513–1515 (2009).
2. Schwaneck, A. S. *et al.* Broken time reversal of light interaction with planar chiral nanostructures. *Phys. Rev. Lett.* **91,** 247404 (2003).
3. Kuwata-Gonokami, M. *et al.* Giant optical activity in quasi-two-dimensional planar nanostructures. *Phys. Rev. Lett.* **95,** 227401 (2005).
4. Hendry, E. *et al.* Ultrasensitive detection and characterization of biomolecules using superchiral fields. *Nature Nanotech.* **5,** 783–787 (2010).
5. Slocik, J. M., Govorov, A. O. & Naik, R. R. Plasmonic circular dichroism of peptide functionalized gold nanoparticles. *Nano. Lett.* **11,** 701–705 (2011).
6. George, J. & Thomas, K. G. Surface plasmon coupled circular dichroism of Au nanoparticles on peptide nanotubes. *J. Am. Chem. Soc.* **132,** 2502–2503 (2010).
7. Shukla, N., Bartel, M. A. & Gellman, A. J. Enantioselective separation on chiral Au nanoparticles. *J. Am. Chem. Soc.* **132,** 8575–8580 (2010).
8. Řezanka, P., Záruba, K. & Král, V. Supramolecular chirality of cysteine modified silver nanoparticles. *Colloids Surf. A* **374,** 77–83 (2011).
9. Elemans, J. A. A. W., de Cat, I., Xu, H. & de Feyter, S. Two-dimensional chirality at liquid–solid interfaces. *Chem. Soc. Rev.* **38,** 722–736 (2009).
10. Ernst, K. H. *Supramolecular Surface Chirality* 209–252 (Springer, 2006).
11. Ernst, K. H. Molecular chirality in surface science. *Surf. Sci.* **613,** 1–5 (2013).
12. Chon, H., Lee, S., Son, S., Oh, C. H. & Choo, J. Highly sensitive immunoassay of lung cancer marker carcinoembryonic antigen using surface-enhanced Raman scattering of hollow gold nanospheres. *Anal. Chem.* **81,** 3029–3034 (2009).
13. Camden, J. P., Dieringer, J. A., Zhao, J. & van Duyne, R. P. Controlled plasmonic nanostructures for surface-enhanced spectroscopy and sensing. *Acc. Chem. Res.* **41,** 1653–1661 (2008).
14. Temur, E., Boyaci, I., Tamer, U., Unsal, H. & Aydogan, N. A highly sensitive detection platform based on surface-enhanced Raman scattering for *Escherichia coli* enumeration. *Anal. Bioanal. Chem.* **397,** 1595–1604 (2010).
15. Jackson, J. B., Westcott, S. L., Hirsch, L. R., West, J. L. & Halas, N. J. Controlling the surface enhanced Raman effect via the nanoshell geometry. *Appl. Phys. Lett* **82,** 257–259 (2003).
16. Lin, A. W. H., Lewinski, N. A., Lee, M. & Drezek, R. A. Reflectance spectroscopy of gold nanoshells: computational predictions and experimental measurements. *J. Nanopart. Res.* **8,** 681–692 (2006). .
17. Rocks, L., Faulds, K. & Graham, D. Rationally designed SERS active silica coated silver nanoparticles. *Chem. Commun.* **47,** 4415–4417 (2011).
18. Barron, L. D., Hecht, L., Blanch, E. W. & Bell, A. F. Solution structure and dynamics of biomolecules from Raman optical activity. *Prog. Biophys. Mol. Biol.* **73,** 1–49 (2000).
19. Freedman, T. B., Nafie, L. A. & Keiderling, T. A. Vibrational optical activity of oligopeptides. *Biopolymers* **37,** 265–279 (1995).
20. Nafie, L. A. Vibrational optical activity. *Appl. Spectrosc.* **50,** 14A–26A (1996).
21. Berova, N. *et al.* in *Circular Dichroism: Principles and Application* (eds Barron, L. D. & Hecht, L.) 667–702 (Wiley-VCH, 2000).
22. Barron, L. D., Hecht, L., McColl, I. H. & Blanch, E. W. Raman optical activity comes of age. *Mol. Phys.* **102,** 731–744 (2004).
23. Adachi, K. *et al.* Chirality induction and amplification in methylene blue H-aggregates via D- and L-phenylalanine pre-adsorbed on the tungsten oxide nanocolloid surface. *New J. Chem.* **36,** 2167–2170 (2012).
24. Angeluts, A. A. *et al.* Second harmonic generation upon reflection of light from the surface of a solution of mirror-asymmetric molecules: a new tool for studies of molecular chirality. *Opt. Spectrosc.* **87,** 151–156 (1999).
25. Borovkov, V. V., Lintuluoto, J. M., Fujiki, M. & Inoue, Y. Temperature effect on supramolecular chirality induction in bis(zinc porphyrin). *J. Am. Chem. Soc.* **122,** 4403–4407 (2000).
26. Borovkov, V. V., Yamamoto, N., Lintuluoto, J. M., Tanaka, T. & Inoue, Y. Supramolecular chirality induction in bis(zinc porphyrin) by amino acid derivatives: rationalization and applications of the ligand bulkiness effect. *Chirality* **13,** 329–335 (2001).
27. Chilaya, G. Induction of chirality in nematic phases. *Rev. Phys. Appl.* **16,** 193–208 (1981).
28. Chavan, S. P. & Khatod, H. S. Enantioselective synthesis of the essential oil and pheromonal component ar-himachalene by a chiral pool and chirality induction approach. *Tetrahedron: Asymmetry* **23,** 1410–1415 (2012).
29. Fireman-Shoresh, S., Marx, S. & Avnir, D. Induction and detection of chirality in doped sol–gel materials: NMR and circular dichroism studies. *J. Mater. Chem.* **17,** 536–544 (2007).
30. Ostovar pour, S., Bell, S. E. J. & Blanch, E. W. Use of a hydrogel polymer for reproducible surface enhanced Raman optical activity (SEROA). *Chem. Commun.* **47,** 4754–4756 (2011).
31. Abdali, S. & Blanch, E. W. Surface enhanced Raman optical activity (SEROA). *Chem. Soc. Rev.* **37,** 980–992 (2008).
32. Etchegoin, P. G., Galloway, C. & Le Ru, E. C. Polarization-dependent effects in surface-enhanced Raman scattering (SERS). *Phys. Chem. Chem. Phys.* **8,** 2624–2628 (2006).
33. Barron, L. D. *Molecular Light Scattering and Optical Activity* (Cambridge Univ. Press, 2004).
34. Nafie, L. A. Theory of resonance Raman optical activity: The single electronic state limit. *Chem. Phys.* **205,** 309–322 (1996).
35. Nafie, L. A. *Vibrational Optical Activity: Principles and Applications* (Wiley, 2011).
36. Abdali, S., Johannessen, C., Nygaard, K. & Nørbygaard, T. Resonance surface enhanced Raman optical activity of myoglobin as a result of optimized resonance surface enhanced Raman scattering conditions. *J. Phys. Condens. Matter* **19,** 285205 (2007).
37. Abdulrahman, N. A. *et al.* Induced chirality through electromagnetic coupling between chiral molecular layers and plasmonic nanostructures. *Nano. Lett.* **12,** 977–983 (2012).
38. Cao, T. *et al.* A comparison of the chiral counterion, solvent, and ligand used to induce a chiroptical response from Au25 nanoclusters. *Nanoscale* **5,** 7589–7595 (2013).
39. Liu, M. *et al.* Spontaneous chiral symmetry breaking in metamaterials. *Nature Commun.* **5,** 4441 (2014).

40. Iski, E. V., Tierney, H. L., Jewell, A. D. & Sykes, E. C. H. Spontaneous transmission of chirality through multiple length scales. *Chem. Eur. J.* **17,** 7205–7212 (2011).
41. Fabrikanos, V. A., Athanassiou, S. & Lieser, K. Dastelung stabiler hydrosole von gold und silber durch reduktion mit athylendiamintetraessingsaure. *Z. Naturforsch. B* 612–616 (1963).
42. Becke, A. D. Density-functional thermochemistry. III. The role of exact exchange. *J. Chem. Phys.* **98,** 5648–5652 (1993).
43. Frisch, M. J. *et al. Gaussian 09, Revision D01* (Gaussian, 2009).
44. Marenich, A. V., Cramer, C. J. & Truhlar, D. G. Universal solvation model based on solute electron density and on a continuum model of the solvent defined by the bulk dielectric constant and atomic surface tensions. *J. Phys. Chem. B* **113,** 6378–6396 (2009).
45. Novák, V., Šebestík, J. & Bouř, P. Theoretical modeling of the surface-enhanced Raman optical activity. *J. Chem. Theory Comput.* **8,** 1714–1720 (2012).

Acknowledgements

This work was supported by the UK Engineering and Physical Sciences Research Council (EP/P504325/1 and GR/S75727/01), the Royal Society of Chemistry Analytical Sciences Division Studentship Scheme (GR/T05554/01), the Academy of Sciences (M200551205), and the Grant Agency (P208/11/0105, 13-03978S) of the Czech Republic.
The authors thank E. Smith, M. Kadodwala, E. Hendry, C. Johannessen, S. Webb and A. Doig for discussions and D.G. acknowledges the Royal Society for support from a Wolfson research merit award.

Author contributions

E.B. directed the project. D.G. and K.F. led the nanoparticle preparation and characterization. P.B. led the computational modelling. S.O.P. performed the SERROA studies. S.O.P. and L.R. performed SERS and characterization experiments. V.P. performed computational modelling. All authors contributed to preparing the manuscript, with E.B. and S.O.P. being the main authors.

Additional information

Supplementary information is available in the online version of the paper. Reprints and permissions information is available online at www.nature.com/reprints. Correspondence and requests for materials should be addressed to P.B. and E.W.B.

Competing financial interests

The authors declare no competing financial interests.